Processing and Application of Ceramics 16 [3] (2022) 218–229

https://doi.org/10.2298/PAC2203218G

The effect of Sr and Mg substitutions on structure, mechanical properties and solubility of fluorapatite ceramics for biomedical applications

Mohammad Hossein Ghaemi[1,*], Sergiy Y. Sayenko[2], Volodymyr Shkuropatenko[2], Anna Zykova[2], Kateryna Ulybkina[2], Olena Bereznyak[2], Andrzej Krupa[3], Mirosław Sawczak[3]

[1]*Gdansk University of Technology, G. Narutowicza 11/12, 80-233, Gdansk, Poland*
[2]*NSC Kharkov Institute Physics & Technology NASU, 1, Akademicheskaya St., Kharkov, 61-108, Ukraine*
[3]*Institute of Fluid-Flow Machinery, Polish Academy of Science, ul. J. Fiszera, 14, 80-952, Gdansk, Poland*

Received 15 September 2021; Received in revised form 14 February 2022; Accepted 6 August 2022

Abstract

Ionic substitutions play important role in the modifications of biological apatites. Recently, the attention has been focused on the co-doping effects on functional properties of apatite based biomaterials. In this research work, the dense samples of fluorapatites, $Ca_{10}(PO_4)_6F_2$ and $Ca_8MgSr(PO_4)_6F_2$, were produced after sintering at 1250 °C for 6 h in air. Structural characterization, carried out with XRD, IR, Raman and SEM, confirmed the formation of dense and homogeneous structure with main fluorapatite and small amount of $Ca_3(PO_4)_2$ phase. The presented results also demonstrate the stability of structural and mechanical properties of fluorapatites after immersion tests in saline and buffer solutions. The durability of mechanical properties and biocompatibility of the $Ca_{10}(PO_4)_6F_2$ and $Ca_8MgSr(PO_4)_6F_2$ fluorapatites make these materials highly attractive for biomedical application.

Keywords: *fluorapatites, Sr/Mg-doping, structure, mechanical properties, solubility, biocompatibility*

I. Introduction

Minerals and synthetic compounds with a structural type of apatite are widely used in many fields, including construction and electronic industries. Such materials also serve as catalysts and ion exchangers in the chemical industry. Apatites activated by rare earth elements are used as luminescent and laser materials. Moreover, apatite materials are considered as promising materials for immobilization of high-level waste (HLW) due to high chemical and radiation resistance and a wide range of structural iso- and heterovalent substitutions [1,2]. Some types of apatite materials have found wide application in orthopaedics and dentistry due to the composition close to inorganic components of human bones and teeth [3–5].

Biological apatites, including hydroxyapatite ($Ca_{10}(PO_4)_6(OH)_2$, HAp), have been widely used in the biomedical field due to their bioactivity, biocompatibility and osteoconductive properties [6]. Recently, a large number of attempts have been made to modify properties of biological apatites properties, such as biocompatibility, mechanical properties and solubility. Natural apatites contain various amounts of substitutions (F^-, CO_3^{2-}, Sr^{2+}, Mg^{2+}, Zn^{2+}) [7–9]. Fluorine-substituted HAp ($Ca_{10}(PO_4)_6(OH)_xF_{2-x}$, FHAp) and fluorapatite ($Ca_{10}(PO_4)_6F_2$, FAp) have low solubility and good biocompatibility [10,11]. The incorporation of fluorine into apatite lattice makes it apatite structure more stable and a quite well-ordered apatite structure can be formed [12]. Fluorine replacement can favour the crystallization of calcium phosphate, improve the chemical stability and decrease the mineral dissolution [13,14]. In addition, substitution of OH^- groups by F^- results in a better protein adsorption and cell attachment [15]. Fluoride in saliva and blood plasma is necessary for dental and skeletal development and plays a very important role in stimulating the processes of proliferation and differentiation of bone cells. The osteoblast responses were improved through fluoride incorporation [16].

---

[*] Corresponding author: tel: +48 602342507
e-mail: *ghaemi@pg.edu.pl*

Despite the fact that apatites are widely proposed as biocompatible and osteoconductive materials, they demonstrate some principal limitations for long-term clinical applications. A large number of studies have been made to enhance their mechanical properties, such as brittleness and mechanical strength. Thus, it is shown that the ionic substitutions in biological apatites play a key role in enhancing such functional properties as biocompatibility and mechanical strength [17–19].

Strontium, a trace element chemically close to calcium, is mainly incorporated into bone by two mechanisms: surface exchange or ionic substitution. Bone mineral consists of a poorly crystalline fraction made of apatite and calcium phosphate complexes. The strontium levels in bone change in accordance with the bone structure. Furthermore, at the crystal level, higher Sr concentrations are observed in newly formed bone than in old bone [20].

There is experimental evidence that strontium induces pharmacological actions in bone metabolism [21,22]. The strontium ability to substitute calcium in the hydroxyapatite crystal lattice has been previously demonstrated [23]. Sr has also been incorporated in the structure of new bioactive materials, and is used as a drug in the form of strontium ranelate to increase the densification of bone in osteoporotic patients. *In vivo* studies of Sr bioactive glasses [24] have shown that strontium has a dual function within bone remodelling. It is able to uncouple the process of bone resorption and bone formation by inhibiting osteoclasts and stimulating osteoblasts, respectively. Sr substituted calcium phosphate cements/ceramics were used in orthopaedic, in filling bone defects [25]. The composite materials with 1 wt.% SrO added to biogenic hydroxyapatite (HAp) or hydroxyapatite of biogenic origin (BHAp) have been proposed by Kuda *et al.* [26]. It was found that BHAp/glass/SrO composite possessed a higher porosity and rate of dissolution in a physiologic solution. A beneficial effect of low doses of stable strontium in the treatment of osteoporosis age-related bone diseases was reported. The strontium-induced increase of bone formation results in a better mechanical resistance of bones. The Sr-doped ceramic materials were considered for the development of coatings or composite biomaterials to expand the range of biomedical applications [26].

In turn, magnesium is one of the most important cationic substitutes for calcium in biological apatites. Dentin, enamel and bone contain 1.23, 0.44 and 0.72 wt.% of Mg, respectively. Over 100 enzymes require the presence of Mg^{2+} ions for their catalytic actions. These facts make Mg one of the essential elements for all living organisms [27]. Magnesium is closely related with the mineralization of calcified tissue and indirectly influences mineral metabolism [28]. Magnesium deficiency affects all skeletal metabolism stages such as bone growth and bone fragility [29]. Fluorine-substituted HAp, FAp, and Mg-substituted apatites have received increasing attentions in the field of biomedicine. Mg^{2+} substituted FAp provides greater biocompatibility and better biological properties than the pure FAp or HAp. The formation and attachment of biomimetic Ca-P coatings in the simulated body fluid (SBF) solution were strongly related to Mg^{2+} content, where Mg-substitution improves the bioactivity of apatite in SBF [13]. In addition, Mg ion promotes bone-like apatite nucleation and growth on titanium surface in SBF solution and improves MC3T3-E1 (E1 type of MC3T3 is an osteoblast precursor cell line derived from Mus musculus of mouse calvaria) cell proliferation [30].

On the other hand, recently the attention has been focused on the co-doping effects of additives on the chemical dissolution behaviour of biomaterials. Melt-derived Sr-containing polyphosphate glasses, doped with Mg and Ti were investigated by Weiss *et al.* [31]. The inclusion of Mg and Ti was found to increase the bonding strength between phosphate chains resulting in a higher stiffness, better mechanical properties, and lower degradation rates in buffer solution. The properties of different melt-derived alkali-free phosphosilicate glass compositions co-doped with Zn^{2+} and Sr^{2+} ions were also investigated [32]. The compounds showed lower solubility as a result of the ionic field strength associated with its constituent ions. There was a significant difference in the leaching of Zn^{2+} and Sr^{2+} ions in SBF and buffer solution, with a higher rate of release for Sr. Additionally, the substitution of SrO with CaO led to the partial replacement of Ca^{2+} by Sr^{2+} in the fluorapatite and diopside crystal structures [33].

The effect of Sr and Mg substitutions in melt-derived glasses system of $CaO-P_2O_5-Na_2O$ was investigated by Stefanic *et al.* [34]. The chemical durability of glasses in water was found to decrease with decreasing Sr content, and it was characterized by linear degradation and highly controllable profiles. The incorporation of Sr and Mg ions improve the solubility, bioactivity and mechanical properties of the glass-ceramics composite system. It was demonstrated that most Mg ions remained in the glass matrix and had a negative effect on the crystallization of apatite with a high Ca/P ratio. On the other hand, the presence of Sr element was detected in all the deposited apatites, indicating that the introduced strontium was capable to substitute into the formed apatite nuclei and favour the formation of apatite crystallization.

The effects of both doping amount and sintering conditions on the bioceramics properties were investigated in some studies [35–37]. Magnesium and strontium were tested with the aim to compare co-doping effects and benefits of both cations on the process of phase stabilization of tricalcium phosphate (β-TCP) structure [38,39]. The additions of SrO and MgO in TCP resulted in smaller grain size, increased density and pore size reduction that was beneficial for the mechanical properties of TCP biomaterials [40]. The improvement of mechanical and biological properties of Mg-Sr co-doped TCP materials was previously analysed by *in vivo* study [41].

In addition to biocompatible properties of calcium phosphate ceramics, the antibacterial effect of Sr and Mg substitution has not been well-understood and is an open issue of research. *In vitro* antibacterial activity and cytocompatibility were investigated [42,43]. The optimal balance between antibacterial activity and cytocompatibility was detected by the presence of MgO in HAp/MgO structure. The MgO additives resulted in the significant reduction of bacterial proliferation. The angiogenic and inflammation potentials were also confirmed by *in vivo* tests. The granules containing MgO stimulated angiogenesis without increasing inflammation. The dual effect of MgO additives was shown. The inclusion of MgO reduced bacterial growth and biofilm formation in a HAp-based bone substitution.

On the other hand, an inhibitory effect of Sr additives on various strains such as *Escherichia Coli* (*E. coli*) and *Porphyromonasgingivalis* (*P. gingivalis*) was also investigated [44]. Brauer *et al.* [45] showed that the bactericidal action of bone cements was increased via Sr substitution. The samples containing small amounts of Sr (2.5 mol%) reduced the number of bacteria (*Streptococcus faecalis*) up to one order of magnitude as compared to Sr-free samples. In addition, fluorine ions are known to affect the mineralization and bone formation *in vivo*, resulting in their antibacterial effect. It can be concluded that Sr^{2+} and Mg^{2+} ions have a synergistic effect with F^- ions in promoting the antibacterial activity.

Mg and Sr substituted phosphate ceramics and glasses are very attractive materials for the production of modern implants, prosthesis for orthopaedic, dental surgery and scaffolds for tissue engineering applications [46]. However, the effects of thermal treatment and sintering condition on the mechanical properties and dissolution behaviour of such co-doped compositions are not so well studied. It is well-known that the dissolution of ceramics in biological environment is complex and depends on numerous factors, such as phase composition, density, and surface parameters. Thus, a further focus on the effect of Sr and Mg co-doping on structure, mechanical properties and solubility of calcium phosphate ceramics is of great interest and is subject of this work.

II. Experimental

2.1. Sample preparation

The pure and Sr-Mg-doped fluorapatite powders ($Ca_{10}(PO_4)_6F_2$ and $Ca_8MgSr(PO_4)_6F_2$) were prepared by chemical co-precipitation method, previously described in the literature [2]. The following components were used: calcium nitrate ($Ca(NO_3)_2 \cdot 4\,H_2O$, Alchim, Ukraine), diammonium phosphate ($(NH_4)_2HPO_4$, Alchim, Ukraine), ammonium fluoride (NH_4F, Alchim, Ukraine), strontium nitrate ($Sr(NO_3)_2$, Alchim, Ukraine) and magnesium nitrate ($Mg(NO_3)_2$, Alchim, Ukraine), which were taken in stoichiometric proportions. The used chemical co-precipitation method included the following stages: i) preparation of aqueous solutions of the initial components with the required concentrations, ii) mixing of initial solutions, iii) adjusting pH to 9–9.5 by the addition of NH_4OH and precipitation of $Ca_{10}(PO_4)_6F_2$ and $Ca_8MgSr(PO_4)_6F_2$ powders and iv) decantation, washing, drying in air and grinding.

Samples for sintering were prepared in the form of pellets with a diameter of 14 mm and a height of 5–7 mm made by cold uniaxial pressing of synthesized fluorapatite powders on a hydraulic press within pressure range of 124–247 MPa. Sintering of the fluorapatite samples was carried out in a Nabertherm GmbH L5/13/B180 furnace. In order to produce fluorapatite structures with higher density, the samples were sintered in the temperature range 1000–1250 °C for 6 h in air.

2.2. Characterization

In order to assess the thermal behaviour of the produced powders, differential thermal analysis (DTA) and thermogravimetric analysis (TGA) experiments were carried out using a SDT Q600 V20.9 Build 20 Thermal analyser.

Phase compositions of the synthesized powders and sintered ceramics were studied by X-ray diffraction (XRD) analysis on a DRON-4-07 using copper anode. Transmission electron microscopy (TEM) images of the fluorapatite powders were made by TEM 123K microscope (Hitachi, Japan). The microstructure and chemical composition of the obtained ceramic materials were analysed by scanning electron microscopy (SEM) and energy dispersive X-ray (EDX) spectroscopy (Zeiss Evo-40). The apparent density (ρ_{ap}) of the sintered samples was determined by hydrostatic weighing method. FTIR spectrometer IRS-29 (LOMO) was used to record absorption spectra in the IR range. The spectra were detected in the spectral range 4000–400 cm^{-1} (mid-infrared region). Raman spectra were analysed by a Raman spectroscopy method on confocal microscope (Renishaw inVia).

Mechanical properties tests of the fluorapatite samples for evaluation of Vickers hardness and elastic modulus were performed by nanoindentation method on a NanoIndenter G200. The average values were evaluated as result of 10 indents at a depth of 1 µm on the sample surface. Fracture toughness K_{IC} was determined by using Vickers indentation and the following formula [63]:

$$K_{IC} = \frac{0.203 \cdot H \cdot \sqrt{a}}{\left(\frac{c}{a}\right)^{1.5}} \tag{1}$$

where c is the radial crack dimension measured from the centre of the indent impression, a is the half diagonal of the indentation and H is the hardness.

The dissolution tests of the fluorapatite samples were carried out by immersion them in saline and sodium phosphate buffer solution (NaCl - 8, KCl - 0.2, Na_2HPO_4 - 1.44, KH_2PO_4 - 0.24 g/l, pH = 7.4) at 37 °C. After 1, 3, 7 and 14 days of testing, the samples were weighed and the weight losses divided by the total surface of the sample ($\Delta w/S$, mg/dm^2) were determined. The fractured surfaces were observed by SEM and laser confocal microscope methods (Olympus Lext OLS4100) after immersion tests.

III. Results and discussion

3.1. Characterization of synthesized powders

XRD results of the pure and Sr-Mg-doped fluorapatite powders ($Ca_{10}(PO_4)_6F_2$ and $Ca_8MgSr(PO_4)_6F_2$), obtained by co-precipitation method, are shown in Fig. 1. It can be seen that single-phase fluorapatites with $Ca_{10}(PO_4)_6F_2$ (Fig. 1a) and $Ca_8MgSr(PO_4)_6F_2$ structures (Fig. 1b) without any secondary phase were produced. Ionic radius of Sr^{2+} (1.13 Å) is slightly bigger, whereas ionic radius of Mg^{2+} (0.65 Å) is significantly smaller than Ca^{2+} (0.99 Å) [48]. These all indicate that Sr^{2+} and Mg^{2+} are incorporated in fluorapatite lattice. The substitutions of Ca^{2+} by Sr^{2+} and Mg^{2+} ions in the synthesized $Ca_{10}(PO_4)_6F_2$ powders leaded to the increase of fluorapatite lattice parameters from a = 9.350 Å and c = 6.870 Å to a = 9.393 Å and c = 6.894 Å.

It can also be seen from Fig. 1 that the corresponding XRD peaks are relative broad for both $Ca_{10}(PO_4)_6F_2$ and $Ca_8MgSr(PO_4)_6F_2$ powders indicating on small sizes of coherent scattering regions (crystallites), being in the range of 30–33 nm. These results are in good agreement with the literature data [47]. Transmission electron microscopy (TEM) images (Fig. 2) reveal that the fluorapatite powders synthesized by chemical co-precipitation method are agglomerated and mainly consist of the nanocrystalline particles with the average particle size of 20–30 nm for the sample $Ca_{10}(PO_4)_6F_2$ (Fig. 2a) and somewhat larger particles in the case of the $Ca_8MgSr(PO_4)_6F_2$ powders (Fig. 2b).

Differential thermal and thermogravimetric analyses (DTA/TGA) curves of the $Ca_{10}(PO_4)_6F_2$ and $Ca_8MgSr(PO_4)_6F_2$ powders produced by chemical co-precipitation method have a similar character (Fig. 3). The obtained data indicate the presence of two thermal effects. The first one relates to the removal of adsorbed water at temperature of ~60–110 °C. The second may be associated with the thermal decomposition of fluorapatites according to the following reaction [49]:

$$Ca_{10}(PO_4)_6F_2 \longrightarrow 3\,Ca_3(PO_4)_2 + CaF_2 \qquad (2)$$

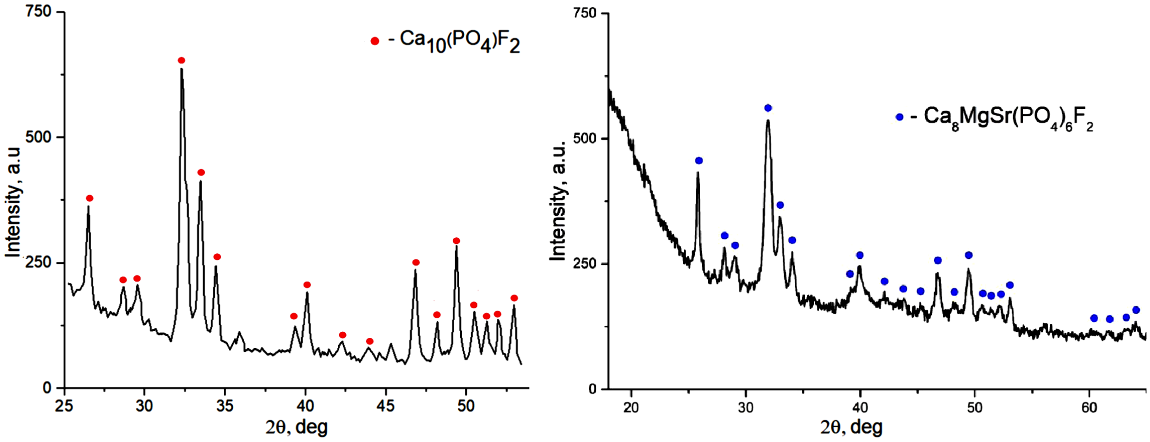

Figure 1. XRD patterns of synthesized powders: a) $Ca_{10}(PO_4)_6F_2$ and b) $Ca_8MgSr(PO_4)_6F_2$

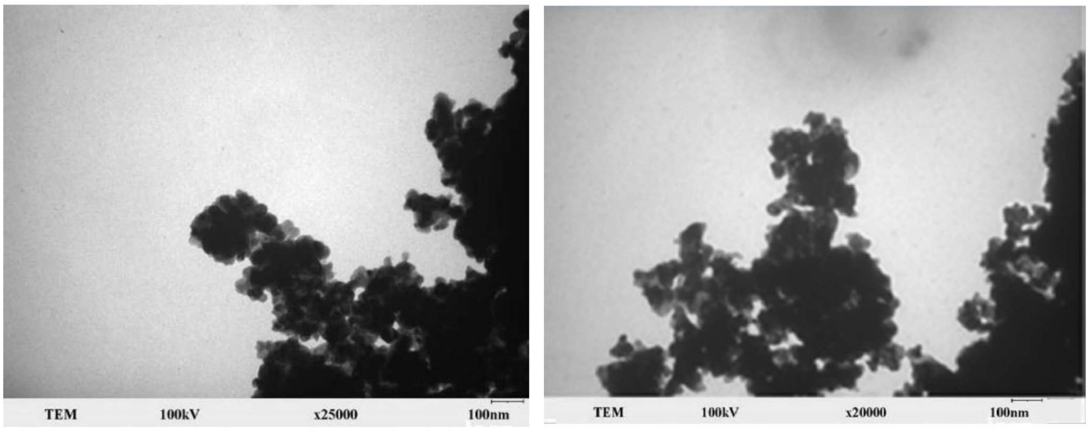

Figure 2. Transmission electron microscopy (TEM) of $Ca_{10}(PO_4)_6F_2$ (a) and $Ca_8MgSr(PO_4)_6F_2$ (b) powders obtained by chemical co-precipitation

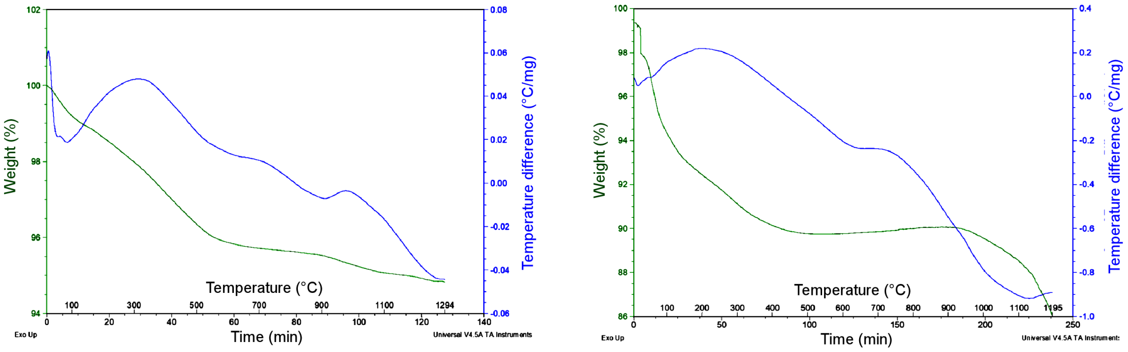

Figure 3. DTA/TGA curves of: a) $Ca_{10}(PO_4)_6F_2$ and b) $Ca_8MgSr(PO_4)_6F_2$ samples

For the pure fluorapatite (sample $Ca_{10}(PO_4)_6F_2$), the partial decomposition temperature is near 900 °C (Fig 3a), whereas it decreases to 650 °C when Ca^{2+} is replaced by Sr^{2+} and Mg^{2+} (Fig. 3b).

3.2. *Characterization of sintered ceramics*

Phase compositions of the sintered (1250 °C, 6 h) fluorapatite and Sr-Mg-doped fluorapatite samples are represented by the main fluorapatite phases (i.e. $Ca_{10}(PO_4)_6F_2$ and $Ca_8MgSr(PO_4)_6F_2$) as it can be seen from Fig. 4. The presence of tricalcium phosphate ($Ca_3(PO_4)_2$) concomitant phase was also observed for both fluorapatite and Sr-Mg-doped fluorapatite samples. However, it should be noted that content of $Ca_3(PO_4)_2$ phase is much higher in the $Ca_8MgSr(PO_4)_6F_2$ (18.4 wt.%.) in comparison with that for the undoped $Ca_{10}(PO_4)_6F_2$ sample. The presence of the higher amount of tricalcium phosphate phase in the sintered Sr-Mg-doped fluorapatite sample is caused by substitution of Ca^{2+} with Mg^{2+} and Sr^{2+} ions and its formation can be accompanied also with the appearance of CaF_2 phase [49] (not detected in XRD pattern shown in Fig. 4).

According to density measurements (ρ_{ap}), it is found that the maximum relative densities of the fluorapatites $Ca_{10}(PO_4)_6F_2$ and $Ca_8MgSr(PO_4)_6F_2$ after sintering at 1250 °C are 92% and 94% (2.95 and 3.14 g/cm^3), respectively. A slight increase in the density of the $Ca_8MgSr(PO_4)_6F_2$ compared to the $Ca_{10}(PO_4)_6F_2$ sample is possibly due to the presence of a some amount of CaF_2 [49] and $Ca_3(PO_4)_2$. As it is known from the phase diagram of calcium fluoride and tricalcium phosphate, an eutectic between CaF_2 and $Ca_{10}(PO_4)_6F_2$ phases is formed near 1200 °C. This effect results in liquid phase formation and might intensify sintering of the $Ca_8MgSr(PO_4)_6F_2$ fluorapatite. Thus, the observed increase of density of the Sr-Mg-doped fluorapatite in comparison to the fluorapatite sample may be related to the liquid phase sintering of the $Ca_8MgSr(PO_4)_6F_2$ fluorapatite.

SEM images of the cleaved fluorapatite samples confirm their homogeneous structure (Fig. 5). As it can be seen, a large number of small pores are present on the cleaved surface of the $Ca_{10}(PO_4)_6F_2$ ceramics while a smaller number of large pores are observed at the $Ca_8MgSr(PO_4)_6F_2$ fractured surface. This difference is attributed to the liquid-phase sintering mechanism activated during the heat treatment of the $Ca_8MgSr(PO_4)_6F_2$ sample at temperature of 1250 °C.

EDX analysis data of the selected sites of cleaved surface of the $Ca_{10}(PO_4)_6F_2$ and $Ca_8MgSr(PO_4)_6F_2$ samples are presented in Fig. 5. The peaks of Ca, P, O, F, Sr and Mg correspond to the peaks of the main fluorapatites elements.

Figure 6 shows IR spectra of the sintered fluorapatite $Ca_{10}(PO_4)_6F_2$ and $Ca_8SrMg(PO_4)_6F_2$ samples. The spectra contain a series of intense bands typical for a fluorapatite-type material. Assignment of these IR

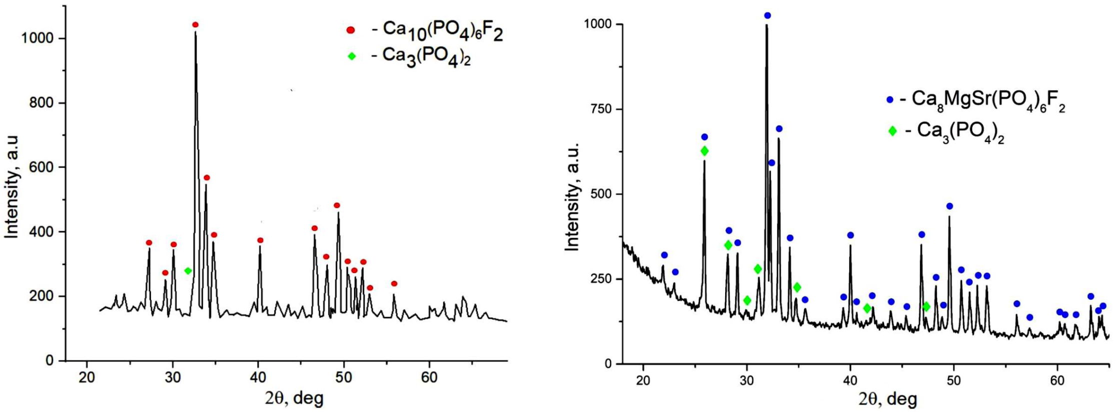

Figure 4. XRD patterns of $Ca_{10}(PO_4)_6F_2$ (a) and $Ca_8MgSr(PO_4)_6F_2$ (b) samples after sintering (1250 °C, 6 h)

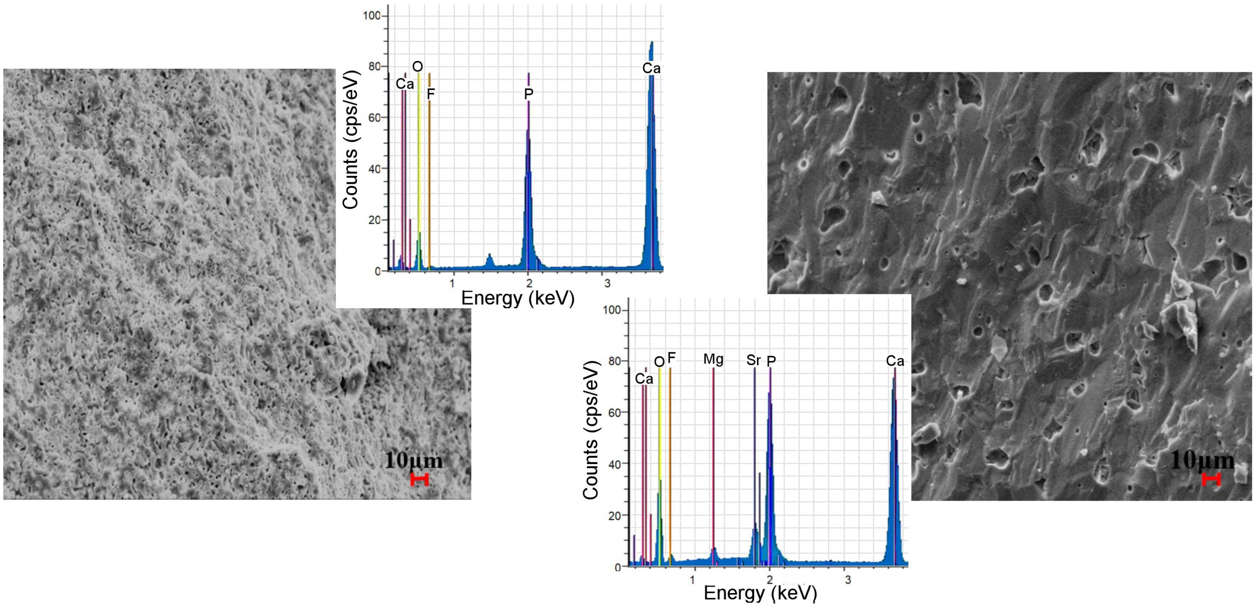

Figure 5. SEM images and elemental compositions (EDS) of fluorapatite samples: a) $Ca_{10}(PO_4)_6F_2$ and (b) $Ca_8MgSr(PO_4)_6F_2$

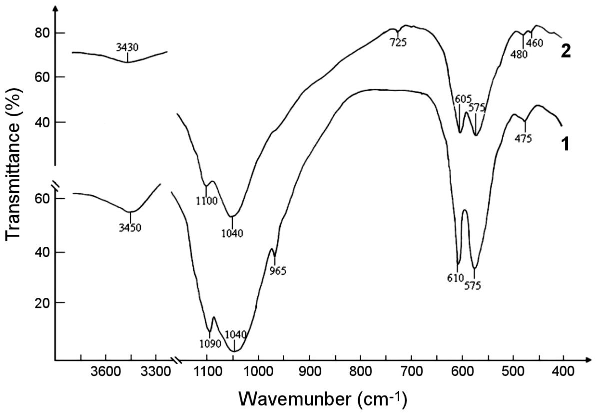

Figure 6. IR absorption spectra of fluorapatites:
1 - $Ca_{10}(PO_4)_6F_2$, 2 - $Ca_8SrMg(PO_4)_6F_2$

bands is given in Table 1. A few differences were observed in the spectrum of the pure and Sr-Mg-doped fluorapatite ceramics. Thus, a characteristic peak of 725 cm^{-1} appears in the doped sample, corresponding to the symmetric vibrations of the bridging bonds of the P–O–P diortho groups, associated to phosphate tetrahedron. In addition, the band in the region of 960 cm^{-1} disappears. This is caused by the degeneracy of the stretching vibrations of PO_4^{3-} ion due to a change in its coordination environment and symmetry due to the breaking of bonds between the phosphate tetrahedron and calcium ions. It was also observed that Sr and Mg doping of fluorapatite results in reduction in the intensity of all bands corresponding to adsorbed water and PO_4^{3-} vibration modes. These facts also suggested that Ca is substituted by Sr and Mg in the fluorapatite lattice.

According to Raman analyses of bone structure [51] it was demonstrated that strontium can be heterogeneously distributed in bone mineral, with a higher amount in newly formed bone tissue than in old bone tissue. Additionally, it was shown that the strontium incorporation does not make any significant change in the crystal lattice parameters.

In our study, in accordance with the infrared spectroscopy analyses, and also Raman spectra (Fig. 7) of the pure and Sr-Mg-doped fluorapatites, internal vibrational modes of PO_4^{3-} group were detected. Thus, the most intense line of the symmetric stretching vibration ν_1 (PO) at 961 cm^{-1}, which is a characteristic value for

Table 1. Assignment of the bands in the IR spectra of fluorapatite samples

IR bands		Description [50]
$Ca_{10}(PO_4)_6F_2$	$Ca_8SrMg(PO_4)_6F_2$	
475 cm^{-1}	460 and 480 cm^{-1}	Vibrations of OH^- groups replacing F^- in apatite structure
575 cm^{-1}	575 cm^{-1}	Bending vibrations of PO_4^{3-} tetrahedra
610 cm^{-1}	605 cm^{-1}	Bending vibrations of PO_4^{3-} tetrahedra
	725 cm^{-1}	Symmetric vibrations of bridging P–O bonds
965 cm^{-1}		Stretching vibrations of PO_4^{3-} tetrahedra
1040 cm^{-1}	1040 cm^{-1}	Stretching vibrations of PO_4^{3-} tetrahedra
1090 cm^{-1}	1100 cm^{-1}	Stretching vibrations of PO_4^{3-} tetrahedra
3450 cm^{-1} (~10%)	3430 cm^{-1} (~5%)	Adsorbed H_2O (stretching vibrations of H–O–H)

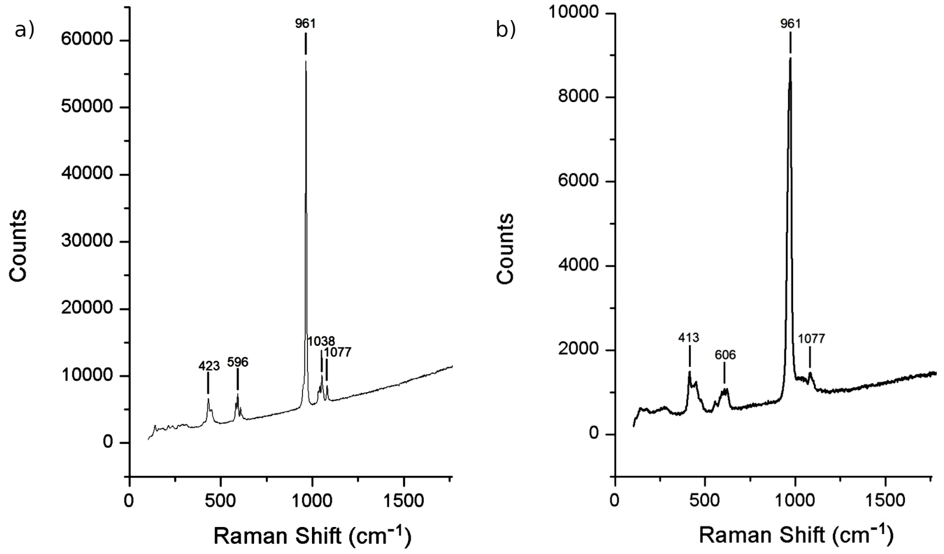

Figure 7. Raman spectra of sintered fluorapatites: a) $Ca_{10}(PO_4)_6F_2$ and b) $Ca_8MgSr(PO_4)_6F_2$

apatites [52,53], is clearly visible. According to the literature data [54], in the case of substitution of phosphate by carbonate ions, the phosphate line ν_1 appears in the range of 955–959 cm^{-1}. The line of symmetric stretching vibration ν_1(PO) was detected at 961 cm^{-1}. This fact indicates the high crystallinity of fluorapatite, which is confirmed by the XRD data (Fig. 4). In addition, the position of the ν_3 line (1038 cm^{-1}), corresponding to the asymmetric P–O stretching vibration, did not change. For the fluorapatite $Ca_8SrMg(PO_4)_6F_2$, a decrease in the intensity of the ν_3 line and its fusion with the extended ν_1 line are observed (Fig. 7b). In contrast to the ν_1 and ν_3 lines, the remaining lines of the P–O deformation vibrations ν_2 (423 → 413 cm^{-1}) and ν_4 (596 → 606 cm^{-1}) are shifted towards lower frequencies when calcium is replaced by Sr and Mg. In addition, on the Raman spectra of the fluorapatite and Sr-Mg-containing fluorapatites, a 1077 cm^{-1} line was observed. This line corresponds to CO_3^{2-} vibrations and indicated partial replacement of phosphate ions by carbonate ions ($CO_3^{2-} \rightarrow PO_4^{3-}$). Inclusion of a small amount of CO_3^{2-} ions in the fluorapatite structure is probably caused by the synthesis conditions and the presence of atmospheric carbon dioxide. It is known that PO_4^{3-} tetrahedron in the fluorapatite lattice is surrounded by 9 Ca^{2+} cations, which isolate it from other PO_4^{3-} tetrahedra. Leroy *et al.* [55] reported that the substitution of PO_4^{3-} by CO_3^{2-} ions does not cause any significant structural changes in the FAp structure that could be observed on the Raman spectra. These results are also in a good agreement with the IR analysis data.

3.3. Immersion tests

Long-term immersion tests demonstrate the real behaviour of the biomaterials in biological environment. In this regard, the solubility of the synthesized fluorapatites in physiological media and the effect of the structural replacement of calcium by strontium and magnesium are of great interest.

The results of the solubility tests of the $Ca_{10}(PO_4)_6F_2$ and $Ca_8MgSr(PO_4)_6F_2$ fluorapatites in saline solution are shown in Fig. 8a. The decrease in degree of fluorapatite solubility with time was observed. These results also indicate a higher degree of solubility of the Sr-Mg substituted fluorapatite in comparison to the undoped fluorapatite. Figure 8b shows the dissolution rate of the synthesized fluorapatites in buffer solution. It should be mentioned that in the previous study [47] an increase

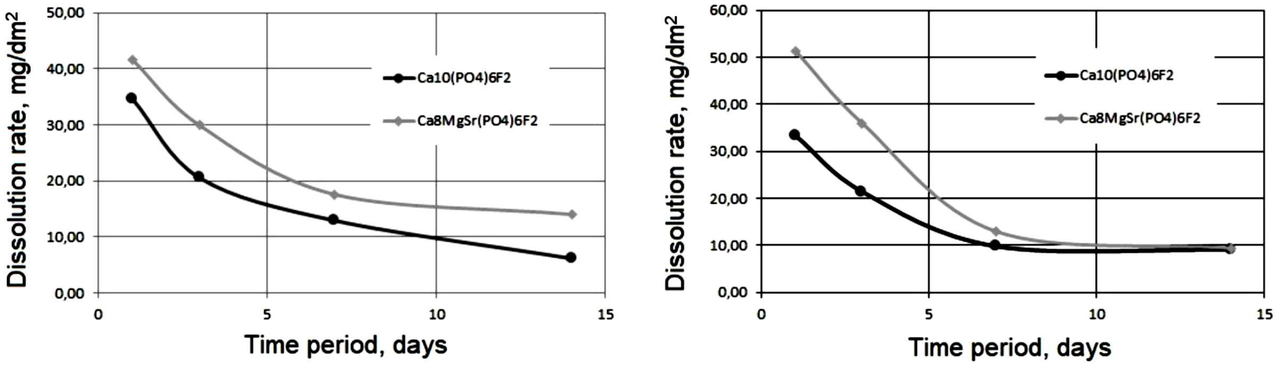

Figure 8. Dissolution rate of $Ca_{10}(PO_4)_6F_2$ and $Ca_8SrMg(PO_4)_6F_2$ fluorapatites in saline (a) and buffer solution (b)

Table 2. Young's modulus, hardness and fracture toughness of fluorapatite samples before and after dissolution tests

Sample	Young modulus [GPa]		Hardness [GPa]		K_{IC} [MPa·m$^{1/2}$]	
	before	after	before	after	before	after
$Ca_{10}(PO_4)_6F_2$	106.3 ± 4.5	97.7 ± 6.1	5.9 ± 1.1	5.2 ± 0.6	2.0 ± 0.9	1.7 ± 0.5
$Ca_8MgSr(PO_4)_6F_2$	102.7 ± 5.3	93.4 ± 4.7	5.5 ± 0.7	4.1 ± 1.9	1.8 ± 0.4	1.3 ± 0.8

of the weight losses and dissolution rates of strontium substituted fluorapatite $Ca_9Sr(PO_4)_6F_2$ in comparison to non-substituted fluorapatite $Ca_{10}(PO_4)_6F_2$ samples was detected. According to Shkuropatenko *et al.* [2], this fact is associated with the presence of $Ca_3(PO_4)_2$ phase in the $Ca_9Sr(PO_4)_6F_2$ samples. It is known that tricalcium phosphate demonstrates greater solubility in comparison with fluorapatite. In contrast, it was reported [56] that the strontium and calcium substitutions cause no principal change in the dissolution rate of phosphate glasses. Additionally, the effect of strontium bonding to a similar number of phosphate chains as calcium was found. The addition of Sr into the phosphate glass composition resulted in a decrease of the dissolution rate of the glass, thus suggesting an increase of the cross-linking between phosphate chains. In the present study, the results demonstrate that in both saline and buffer solutions the solubility of the Sr-Mg substituted fluorapatite is higher than that of the fluorapatite. It should be noted that in buffer solution, the solubility of fluorapatites was not much higher than the solubility in saline solution.

There is a strong correlation between the structure, mechanical properties and solubility of a material. The ceramics with higher density and crystallinity demonstrate better mechanical characteristics and biocompatibility [57]. The hardness to Young's modulus ratio (H/E) is the main parameter, which characterizes the material deformation in relation to yielding [58]. H/E ratio plays an important role in identifying the mechanical behaviours and further brittle failure of ceramic materials and coatings [59]. Furthermore, fracture toughness (K_{IC}) demonstrates the ability of a material to resist against brittle failure and crack propagation. Nanoindentation method allows to make direct measuring of cracks created with a sharp diamond indenter [60,61].

Mechanical properties of the $Ca_8SrMg(PO_4)_6F_2$ and $Ca_{10}(PO_4)_6F_2$ fluorapatites before and after immersion tests are presented in Table 2. As it was previously reported, the presence of MgO particles exhibited lower elastic modulus [62]. The fracture toughness of a material depends on the various parameters, such as: size and properties of phases, grain boundaries, pores. The reduction in the grain size increased the grain-boundary area and the fracture toughness [63]. The strong effect of co-doping with different elements on ion release in apatite structures was previously analysed [64]. Our results show that the measured average value of Young's modulus on the surface of the fluorapatite sample slightly exceeds the value for the Sr-Mg-doped fluorapatite. In addition, after a solubility test in saline solution, the values of Young's modulus measured on the surface of both samples slightly decrease. On the contrary, the decrease of microhardness and K_{IC} is more pronounced for the $Ca_8SrMg(PO_4)_6F_2$ samples after immersion tests possibly due to the higher soluble tricalcium phosphate $Ca_3(PO_4)_2$ phase content. Nevertheless, the dissolution of the fabricated fluorapatites within 14 days occurs to a small extent and does not significantly affect their mechanical properties.

The surface of fluorapatite samples after 14 days of immersion tests in saline solution was studied by Ra-

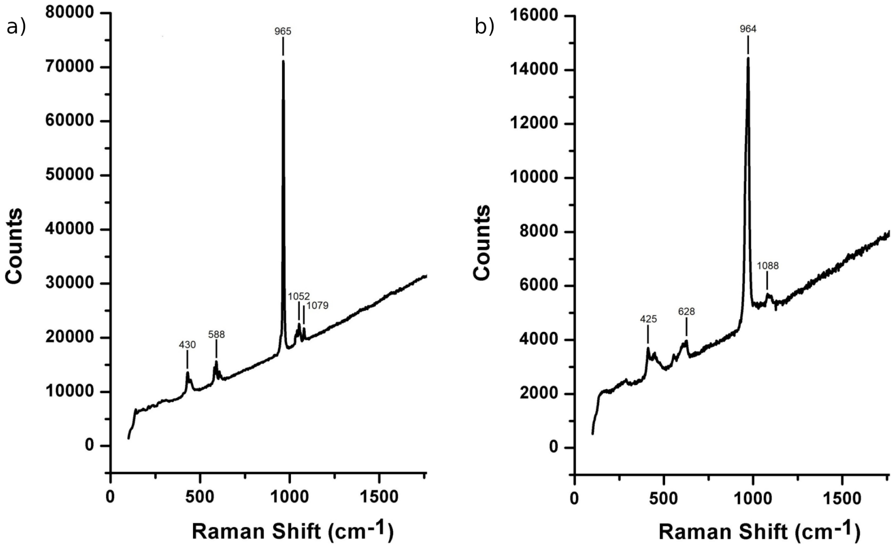

Figure 9. Raman spectra of fluorapatites: a) $Ca_{10}(PO_4)_6F_2$ and b) $Ca_8MgSr(PO_4)_6F_2$ after solubility tests

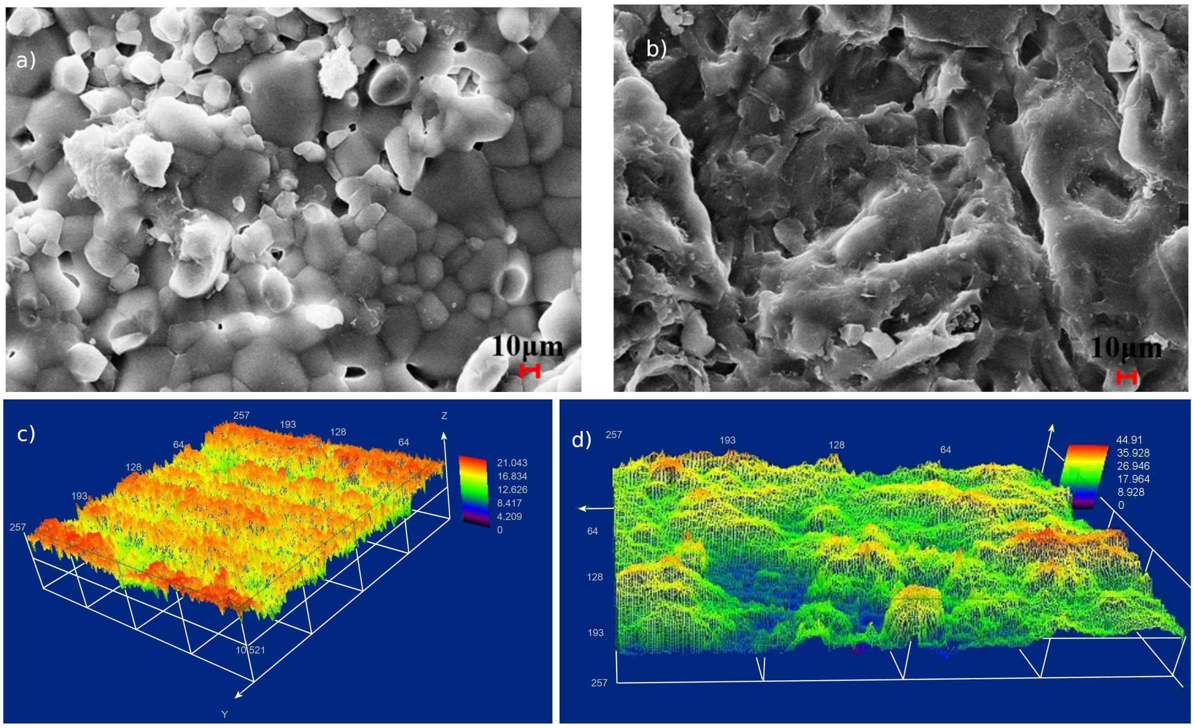

Figure 10. The surface structure and topography of the samples $Ca_{10}(PO_4)_6F_2$ (a, c) and $Ca_8MgSr(PO_4)_6F_2$ (b, d) after immersion tests

man spectroscopy, SEM and laser confocal microscopy. Analysis of the Raman spectra of the surface of the fluorapatite samples after solubility tests also showed the presence of the main fluorapatite lines ν_1(P–O) at 965 cm^{-1} (Fig. 9). These results indicate a strong stability of the fluorapatite and Sr-Mg-doped fluorapatite in saline solution at 37 °C. The presence of ν_1 peak in the Raman spectrum confirms the stability of the fluorapatite crystal structure at the surface of the studied samples. After solubility tests of the $Ca_{10}(PO_4)_6F_2$ fluorapatite, a shift of the ν_3 line (1038 → 1052 cm^{-1}) to the high frequency region and the ν_2 line (423 → 430 cm^{-1}) to lower frequencies were observed (Fig. 9a). On the contrary, the line ν_4 was shifted to the lower frequencies region (596 → 588 cm^{-1}). At the same time, the position of the line corresponding to the vibrations of CO_3^{2-} (1077 → 1079 cm^{-1}) was almost unchanged. For the $Ca_8MgSr(PO_4)_6F_2$ fluorapatite after immersion tests, shift of the lines of P–O deformation vibration ν_2 (413 → 425 cm^{-1}) and ν_4 (606 → 628 cm^{-1}) towards higher frequencies was detected (Fig. 9b). The position of the line corresponding to the vibrations of CO_3^{2-} was also significantly changed (1077 → 1088 cm^{-1}). It is known that the solubility of apatite increases as a result of the replacement of PO_4^{3-} with the CO_3^{2-} ions. The higher solubility of carbonate-containing apatite compared to carbonate-free apatite is partially due to the fact that $Ca^{2+}–CO_3^{2-}$ bonds are weaker than $Ca^{2+}–PO_4^{3-}$ bonds [65].

The presence of the second, more soluble, $Ca_3(PO_4)_2$ phase and partial replacement of phosphorus ions by carbon ions led to the increased solubility level and, ac-

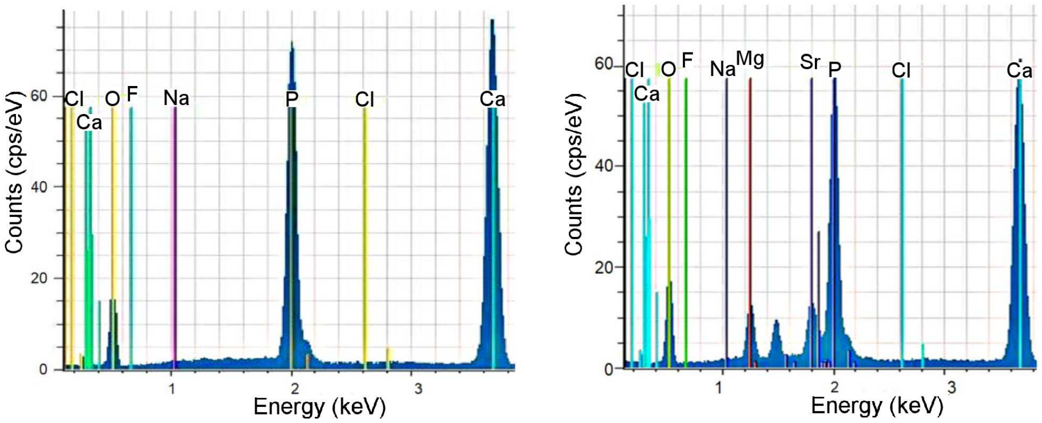

Figure 11. Elemental composition of fluorapatite samples of (a) $Ca_{10}(PO_4)_6F_2$ and (b) $Ca_8MgSr(PO_4)_6F_2$ after dissolution tests

cordingly, to the changes at the surface of fluorapatite samples after dissolution, which are reflected in the Raman spectra.

The surfaces of the $Ca_{10}(PO_4)_6F_2$ and $Ca_8MgSr(PO_4)_6F_2$ samples after immersion tests are significantly different (Figs. 10a,b). It is noticeable that the surface of the $Ca_8MgSr(PO_4)_6F_2$ sample underwent stronger dissolution as compared to the $Ca_{10}(PO_4)_6F_2$ sample (Figs. 10c,d).

It was reported that magnesium influences mineralization both *in vitro* and *in vivo*. The role of magnesium in the formation of Ca-P coatings in the SBF solution was observed. Increase in Mg^{2+} content resulted in the delay of Ca-P precipitation and the structure changed to amorphous or poorly crystallized apatite [66].

According to EDX analysis of the surface after soaking tests, the main peaks of Ca, P, O, F, Sr and Mg corresponding to the elemental composition of fluorapatites are identified in Fig. 11. The EDX spectra demonstrate some changes in the peak intensity after immersion tests. A noticeable decrease of the fluorine content in the composition of the fluorapatites samples was detected. Chaïrat *et al.* [67] argued that the dissolution of apatite is primarily due to the relatively rapid removal of F and Ca from the contact surface. Thus, the destruction of fluorapatite occurs due to the breaking of Ca–O bonds on the surface depleted of calcium and fluorine. On the other hand, the release of low dose of trace elements, such as Sr and Mg demonstrates a beneficial effect and increases bone mass strengthening the bone resorption during bone formation process [68]. A local release of these elements from coatings on metallic implants might improve bone regeneration and have a strong positive impact on clinical applications.

The stability of the structure, phase composition and mechanical properties during long term period of staying in biological environment is very important for biocompatibility of ceramics, if they are used as a biomaterial. Thus, both the $Ca_{10}(PO_4)_6F_2$ and $Ca_8MgSr(PO_4)_6F_2$ fluorapatites can be further proposed as promising candidates for biomedical use in the replacement of defective areas of bone.

IV. Conclusions

In the present study the powders of monophasic fluorapatite ($Ca_{10}(PO_4)_6F_2$) and Sr-Mg doped fluorapatite ($Ca_8MgSr(PO_4)_6F_2$) were obtained by chemical co-precipitation method. The dense fluorapatite samples were produced after sintering at 1250 °C for 6 h in air. Structural characterization, carried out by XRD, IR, Raman and SEM, confirmed the formation of dense and homogeneous structure with main fluorapatite and small amount of $Ca_3(PO_4)_2$ phases. The immersion tests in saline and buffer solutions indicated a greater degree of solubility of the Sr-Mg substituted fluorapatite in comparison to the non-substituted sample. According to scanning electron and laser confocal microscopy analysis, a pronounced surface dissolution of the Sr-Mg doped fluorapatite sample was observed. The mechanical properties of the fluorapatites, such as Young's modulus, hardness and fracture toughness, measured on the surface of the samples slightly decrease for both fluorapatite and Sr-Mg doped fluorapatite after immersion tests.

The results demonstrate stability of structural properties of fluorapatites after soaking in saline and buffer solutions. The durability of mechanical properties and biocompatibility of $Ca_{10}(PO_4)_6F_2$ and $Ca_8MgSr(PO_4)_6F_2$ fluorapatites make these materials highly attractive for biomedical applications.

References

1. O. Terra, F. Audubert, N. Dacheux, C. Guy, R. Podor, "Synthesis and characterization of thorium-bearing britholites", *J. Nuclear Mater.*, **354** (2006) 49–65.
2. V.A. Shkuropatenko, S.Y. Sayenko, K.A. Ulybkina, A.V. Zykova, L.M. Lytvynenko, A.G. Myronova, "Phase composition, structure, corrosion and radiation resistance of synthesized $Ca_{10}(PO_4)_6F_2$ and $Ca_9Sr(PO_4)_6F_2$ fluorapatites", *Funct. Mater.*, **26** [1] (2019) 71–77.
3. S. Ramesha, K.L. Aw, R. Tolouei, M. Amiriyan, C.Y. Tan, M. Hamdi, J. Purbolaksono, M.A. Hassan, W.D. Teng, "Sintering properties of hydroxyapatite powders prepared using different methods", *Ceram. Int.*, **39** (2013) 111–119.
4. E. Landi, A. Tampieri, G. Celotti, S. Sprio, M. Sandri, G. Logroscino, "Sr-substituted hydroxyapatites for osteoporotic bone replacement", *Acta Biomater.*, **3** (2007) 961–969
5. T. Tacail, L. Kovačiková, J. Brůžek, V. Balter, "Spatial distribution of trace element Ca-normalized ratios in primary andpermanent human tooth enamel", *Sci. Total Environmen.*, **603-604** (2017) 308–318.
6. J. Christoffersen, M.R. Christoffersen, N. Kolthoff, O. Barenholdt, "Effects of strontium ions on growth and dissolution of hydroxyapatite and onbone mineral detection", *Bone*, **20** (1997) 47–54.
7. L. Montazeri, J. Javadpour, M.A. Shokrgozar, S. Bonakdar, S. Javadian, "Hydrothermal synthesis and characterization of hydroxyapatite and fluorhydroxyapatite nanosize powders", *Biomed. Mater.*, **5** (2010) 045004.
8. A. Hanifi, M.H. Fathi, H.M. Sadeghi, J. Varshosaz, "Mg^{2+} substituted calcium phosphate nano particles synthesis for non viral gene delivery application", *J. Mater. Sci. Mater. Med.*, **21** (2010) 2393–2401.
9. S. Zhang, Y.S. Wang, X.T. Zeng, K.A. Khor, W. Weng, D.E. Sun, "Evaluation of adhesion strength and toughness of fluoridated hydroxyapatite coatings", *Thin Solid Films*, **516** (2008) 5162–5167.
10. Y. Cai, S. Zhang, X. Zeng, M. Qian, D. Sun, W. Weng, "Interfacial study of magnesium-containing fluoridated hydroxyapatite coatings", *Thin Solid Films*, **519** (2011) 4629–4633.
11. M. Kheradmandfard, M.H. Fathi, M. Ahangarian, E.M Zahrani, "In vitro bioactivity evaluation of magnesium-substituted fluorapatite nanopowders", *Ceram. Int.*, **38** (2012) 169–175.
12. M. Kheradmandfard, M.H. Fathi, "Fabrication and characterization of nanocrystalline Mg-substituted fluorapatite

by high energy ball milling", *Ceram. Int.*, **39** (2013) 1651–1658.

13. Y. Cai, S. Zhang, X. Zeng, Y. Wang, M. Qian, W. Weng, "Improvement of bioactivity with magnesium and fluorine ions incorporated hydroxyapatite coatings via sol–gel deposition on Ti6Al4V alloys", *Thin Solid Films*, **517** (2009) 5347–5351.
14. A. Sharifnabi, M.H. Fathi, B. EftekhariYektaa, M. Hossainalipour, "The structural and bio-corrosion barrier performance of Mg-substituted fluorapatite coating on 316L stainless steel human body implant", *Appl. Surface Sci.*, **288** (2014) 331– 340
15. H.W. Kim, Y.M. Kong, C.J. Bae, Y.J. Noh, H.E. Kim, "Sol-gel derived fluor-hydroxyapatite biocoatings on zirconia substrate", *Biomaterials*, **25** (2004) 2919–2926.
16. B. Basar, A. Tezcaner, D. Keskin, Z. Evis, "Improvements in microstructural, mechanical, and biocompatibility properties of nanosized hydroxyapatites doped with yttrium and fluoride", *Ceram. Int.*, **36** (2010) 1633–1643.
17. L. Cacciotti, "Bivalent cationic ions doped bioactive glasses: the influence of magnesium, zinc, strontium and copper on the physical and biological properties", *J. Mater. Sci.*, **52** (2017) 8812–8831.
18. E. Dietrich, H. Oudadesse, A. Lucas-Girot, Y.L. Gal, S. Jeanne, G. Cathelineau, "Effect of Mg and Zn on the surface of doped melt-derived glass for biomedical applications", *Appl. Surface Sci.*, **255** (2008) 391–395.
19. G.H. Qi, S. Zhang, K.A. Khor, W. Weng, X. Zeng, C. Liu, "In vitro effect of magnesium inclusion in sol-gel derived apatite", *Thin Solid Films*, **516** (2008) 5172–5175.
20. M.D. Grynpas, E. Hamilton, R. Cheung, Y. Tsouderos, P. Deloffre, M. Hott, P.J. Marie, "Strontium increases vertebral bone volume in rats at a low dose that does not induce detectable mineralization defect", *Bone*, **18** (1996) 253–259.
21. Z. Saidak, P.J. Marie, "Strontium signaling: Molecular mechanisms and therapeutic implications in osteoporosis", *Pharmacol. Therapeutics*, **136** (2012) 216–226.
22. P.J. Marie, "Strontium as therapy for osteoporosis", *Curr. Opinion Pharmacol.*, **5** (2005) 633–636.
23. E. Gentleman, Y.C. Fredholm, G. Jell, N. Lotfibakhshaiesh, M.D. O'Donnell, R.G. Hill, M.M. Stevens,, "The effects of strontium-substituted bioactive glasses on osteoblasts and osteoclasts in vitro", *Biomaterials*, **31** (2010) 3949–3956.
24. S. Kargozar, N. Lotfibakhshaiesh, J. Ai, A. Samadikuchaksaraie, R.G. Hill, P.A. Shah, P.B. Milan, M. Mozafari, M. Fathi, M.T. Joghataei, "Synthesis, physico-chemical and biological characterization of strontium and cobalt substituted bioactive glasses for bone tissue engineering", *J. Non-Crystal. Solids*, **449** (2016) 133–140.
25. S. Pina, P. Torres, F. Goetz-Neunhoeffer, J. Neubauer, J. Ferreira, "Newly developed Sr-substituted a-TCP bone cements", *Acta Biomater.*, **6** (2010) 928–935.
26. O. Kuda, N. Pinchuk, O. Bykov, T. Tomila, O. Olifan, M. Golovkova, "Development and characterization of Sr-containing glass-ceramic composites based on biogenic hydroxyapatite", *Nanoscale Res. Lett.*, **13** (2018) 155.
27. A. Saboori, M. Rabiee, F. Moztarzadeh, M. Sheikhi, M. Tahriri, M. Karimi, "Synthesis, characterization and in vitro bioactivity of sol-gel-derived SiO_2-CaO-P_2O_5-MgO bioglass", *Mater. Sci. Eng. C*, **29** (2009) 335–340.
28. W. Mróz, A. Bombalska, S. Burdyn'ka, M. Jedyn'ki, A. Prokopiuk, B. Budner, A. Slósarczyk, A. Zima, E. Menaszek, A. Scisłowska-Czarnecka, K. Niedzielski, "Structural studies of magnesium doped hydroxyapatite coatings after osteoblast culture", *J. Mol. Struct.*, **977** (2010) 145–152.
29. F. Ren, Y. Leng, R. Xin, X. Ge, "Synthesis, characterization and ab initio simulation of magnesium-substituted hydroxyapatite", *Acta Biomater.*, **6** (**2010**) 2787–2796.
30. Y.M. Ko, K. Lee, B.H. Kim, "Effect of Mg ion on formation of bone-like apatite on the plasma modified titanium surface", *Surface Coatings Technol.*, **228** (2013) S404l–S407.
31. D. Weiss, R. Torres, S. Buchner, S. Blunk, P. Soares, "Effect of Ti and Mg dopants on the mechanical properties, solubility, and bioactivity in vitro of a Sr-containing phosphate based glass", *J. Non-Crystal. Solids*, **386** (2014) 34–38.
32. S. Kapoor, A. Goel, A. Tilocca, V. Dhuna, G. Bhatia, K. Dhuna, J.M.F. Ferreira, "Role of glass structure in defining the chemical dissolution behavior, bioactivity and antioxidant properties of zinc and strontium co-doped alkali-free phosphosilicate glasses", *Acta Biomater.*, **10** (2014) 3264–3278.
33. S. Kapoor, A. Goel, M.J. Pascual. J.M. Ferreira, "Thermomechanical behaviour of alkali free bioactive glass-ceramics co-doped with strontium and zinc", *J. Non-Crystal. Solids*, **375** (2013) 74–82.
34. M. Stefanic, M. Peroglio, A.M. Stanciuc, G. Machado, L. Campbell, M.M. Krzmanc, M. Alini, X. Zhang, "The influence of strontium release rate from bioactive phosphate glasses on osteogenic differentiation of human mesenchymal stem cells", *J. Eur. Ceram. Soc.*, **38** (2018) 887–897.
35. D. Veljovic, Z. Radovanovic, A. Dindune, E. Palcevskis, A. Krumina, R. Petrovic, D. Janackovic, "The influence of Sr and Mn incorporated ions on the properties of microwave single- and two-step sintered biphasic HAP/TCP bioceramics", *J. Mater. Sci.*, **49** (2014) 6793–6802.
36. R.K. Chadha, K.L. Singh, C. Sharma, A.P. Singh, V. Naithani, "Effect of microwave and conventional processing techniques on mechanical properties of Strontium substituted hydroxyapatite", *Ceram. Int.*, **46** (2020) 1091–1098.
37. D.J. Curran, T.J. Fleming, M.R. Towler, S. Hampshire, "Mechanical parameters of strontium doped hydroxyapatite sintered using microwave and conventional methods", *J. Mech. Behav. Biomed. Mater.*, **4** (2011) 2063–2073.
38. N. Somers, F. Jean, M. Lasgorceix, H. Curto, G. Urruth, A. Thuault, F. Petit, A. Leriche, "Influence of dopants on thermal stability and densification of β-tricalcium phosphate powders", *Open Ceram.*, **7** (2021) 100168.
39. S.S. Banerjee, S. Tarafder, N.M. Davies, A. Bandyopadhyay, S. Bose, "Understanding the influence of MgO and SrO binary doping on the mechanical and biological properties of β-TCP ceramics", *Acta Biomater.*, **6** (2010) 4167–4174.
40. S. Tarafder, W.S. Dernell, A. Bandyopadhyay, S. Bose, "SrO- and MgO-doped microwave sintered 3D printed tricalcium phosphate scaffolds: Mechanical properties and in vivo osteogenesis in a rabbit model", *J. Biomed. Mater. Res. B Appl. Biomater.*, **103** (2015) 679–690.
41. S. Kannan, F. Goetz-Neunhoeffer, J. Neubauer, S. Pina, P.M.C. Torres, J.M.F. Ferreira, "Synthesis and structural characterization of strontium- and magnesium-co-

substituted β-tricalcium phosphate", *Acta Biomater.*, **6** (2010) 571–576.

42. C.C. Coelho, R. Arajo, P.A. Quadros, S.R. Sousa, F.J. Monteiro, "Antibacterial bone substitute of hydroxyapatite and magnesium oxide to prevent dental and orthopaedic infections", *Mater. Sci. Eng. C*, **97** (2019) 529–538..
43. Y. He, S. Ingudam, S. Reed, A. Gehring, T.P. Strobaugh Jr, P. Irwin, "Study on the mechanism of antibacterial action of magnesium oxide nanoparticles against foodborne pathogens", *J. Nanobiotechnol.*, **14** (2016) 54–61.
44. J. Liu, S.C. Rawlinson, R.G. Hill, F. Fortune, "Strontium-substituted bioactive glasses in vitro osteogenic and antibacterial effects", *Dental Mater.*, **32** (2016) 412–422.
45. D.S. Brauer, N. Karpukhina, G. Kedia, A. Bhat, R.V. Law, I. Radecka, R.G. Hill, "Bactericidal strontium-releasing injectable bone cements based on bioactive glasse", *J. Royal Soc. Interface*, **10** [78] (2013) 20120647.
46. J. Zhang, S. Zhao, Y. Zhu, Y. Huang, M. Zhu, C. Tao, C. Zhang, "Three-dimensional printing of strontium-containing mesoporous bioactive glass scaffolds for bone regeneration", *Acta Biomater.*, **10** (2014) 2269–2281.
47. S.Yu. Sayenko, "Obtaining of strontium doped fluorapatite powders", *Funct. Mater.*, **22** [2] (2015) 263–268.
48. M. Kheradmandfard, M.H. Fathi, F. Ansari, T. Ahmadi, "Effect of Mg content on the bioactivity and biocompatibility of Mg-substituted fluorapatite nanopowders fabricated via mechanical activation", *Mater. Sci. Eng. C*, **68** (2016) 136–142.
49. M.V. Chaikina, "Mechanic chemical processes and the mechanism of energy conversion during indentation of single crystals", *Chem. Sustain. Dev.*, **17** (2009) 653–666.
50. V.C. Farmer, *The Infrared Spectra of Minerals*, Mineralogical Society, London, 1974, 539 p.
51. S.G. Dahl, P. Allain, P.J. Marie, Y. Mauras, G. Boivin, P. Ammann, Y. Tsouderos, P.D. Delmas, C. Christiansen, "Incorporation and distribution of strontium in bone", *Bone*, **28** [4] (2001) 446 –453.
52. C. Garbo, J. Locs, M. D'Este, G. Demazeau, A. Mocanu, C. Roman, O. Horovitz, M. Tomoaia-Cotisel, "Advanced Mg, Zn, Sr, Si multi-substituted hydroxyapatites for bBone regeneration", *Int. J. Nanomed.*, **15** (2020) 1037–1058.
53. Yu. Huaguang, H. Zhang, X. Wang, Z. Gu, X. Li, F. Deng, "Local structure of hydroxyl-peroxy apatite: A combined XRD, FT-IR, Raman, SEM, and solid-state NMR study", *J. Phys. Chem. Solids*, **68** (2007) 1863–1871.
54. C.P. Tarnowski, M.A. Ignelzi Jr, M.D. Morris, "Mineralization of developing mouse calvaria as revealed by Raman microspectroscopy", *J. Bone Mineral Res.*, **17** [6] (2002) 1118–1126.
55. G. Leroy, G. Penel, N. Leroy, E. Bres, "Human tooth enamel: A Raman polarized approach", *Appl. Spectrosc.*, **56** (2002) 1030–1034.
56. U. Patel, R. Moss, K.M.Z. Hossain, A.R. Kennedy, E.R. Barney, I. Ahmed, A.C. Hannon, "Structural and physico-chemical analysis of calcium/strontium substituted, near-invert phosphate based glasses for biomedical applications", *Acta Biomater.*, **60** (2017) 109–127.
57. H.W. Kim, J.C. Knowles, L. Li, H.E. Kim, "Mechanical performance and osteoblast-like cell responses of fluorine-substituted hydroxyapatite and zirconia dense composite", *J. Biomed. Mater. Res. B: Appl. Biomater.*, **70** (2005) 258–268.
58. D.L. Joslin, W.C. Oliver, "A new method for analyzing data from continuous depth-sensing microindentation tests", *J. Mater. Res.*, **5** [1] (1990) 123–126.
59. A. Leyland, A. Matthews, "On the significance of the H/E ratio in wear control: A nanocomposite coating approach to optimised tribological behaviour", *Wear*, **246** [1-2] (2000) 1–11.
60. M.T. Laugier, "New formula for indentation toughness in ceramics", *J. Mater. Sci. Lett.*, **6** (1987) 355–366.
61. B.R. Lawn, "Indentation fracture", pp. 249–306, Ch. 8 in *Fracture of Brittle Solids*, Cambridge University Press, Cambridge, UK, 1993.
62. A. Ricker, P. Liu-Snyder, T.J. Webster, "The influence of nano MgO and $BaSO_4$ particle size additives on properties of PMMA bone cement", *Int. J. Nanomed.*, **3** (2008) 125–132.
63. S. Pazarlioglu, O. Algan, A.M. Isikogullari, H. Gokce, "The effect of lanthanum addition on the microstructure and mechanical properties of Mg-modified hydroxyapatite ceramics", *Process. Appl. Ceram.*, **15** [3] (2021) 226–237.
64. I. Cacciotti, "Multisubstituted hydroxyapatite powders and coatings: the influence of the co-doping on the hydroxyapatite performances", *Int J. Appl. Ceram. Technol.*, **16** [5] (2019) 1864–1884.
65. B. Wopenka, J.D. Pasteris, "A mineralogical perspective on the apatite in bone", *Mater. Sci. Eng. C*, **25** [2] (2005) 131–143.
66. F. Barrere, C.A. van Blitterswijk, K. de Groot, P. Layrolle, "Nucleation of biomimetic Ca–P coatings on Ti6Al4V from a SBF×5 solution: Influence of magnesium", *Biomaterials,* **23** (2002) 2211–2220
67. C. Chaïrat, J. Schott, E.H. Oelkers, J.E. Lartigue, N. Harouiya, "Kinetics and mechanism of natural fluorapatite dissolution at 25 °C and pH from 3 to 12", *Geochim. Cosmochim. Acta*, **71** (2007) 5901–5912.
68. M.D. Grynpas, P.J. Marie, "Effects of low doses of strontium on bone quality and quantity in rats", *Bone*, **11** [5] (1990) 313–319.